

Dynamical models and the phase ordering kinetics of the $s = 1$ spinor condensate

Subroto Mukerjee,^{1,2} Cenke Xu,¹ and J. E. Moore^{1,2}

¹*Department of Physics, University of California, Berkeley, CA 94720*

²*Materials Sciences Division, Lawrence Berkeley National Laboratory, Berkeley, CA 94720*

(Dated: October 26, 2018)

The $s = 1$ spinor Bose condensate at zero temperature supports ferromagnetic and polar phases that combine magnetic and superfluid ordering. We investigate the formation of magnetic domains at finite temperature and magnetic field in two dimensions in an optical trap. We study the general ground state phase diagram of a spin-1 system and focus on a phase that has a magnetic Ising order parameter and numerically determine the nature of the finite temperature superfluid and magnetic phase transitions. We then study three different dynamical models: model A, which has no conserved quantities, model F, which has a conserved second sound mode and the Gross-Pitaevskii (GP) equation which has a conserved density and magnetization. We find the dynamic critical exponent to be the same for models A and F ($z = 2$) but different for GP ($z \approx 3$). Externally imposed magnetization conservation in models A and F yields the value $z \approx 3$, which demonstrates that the only conserved density relevant to domain formation is the magnetization density.

PACS numbers: 03.75.Mn, 03.75.Kk, 64.60.Ht, 75.40.Gb

I. INTRODUCTION

The field of cold atomic gases has witnessed an explosion of experimental and theoretical research in the last ten years. The study of these systems has combined ideas from various disciplines of physics such as atomic physics, condensed-matter physics, optics etc. Cold atomic systems have provided a testing ground for some of the most fundamental principles of collective quantum behavior like Bose-Einstein Condensation. Of particular interest is the study of spinor condensates, which are condensates of atoms with non-zero spin and have been the focus of intense experimental^{1,2,3,4} and theoretical^{5,6,7,8} studies in recent years. The spin degree of freedom opens up the possibility of interesting collective magnetic behavior in these systems in addition to the phenomenon of Bose-Einstein condensation. It has already been demonstrated that the presence of spin greatly modifies the nature of the condensate and superfluid transition in spinor condensates compared to those without spin^{5,9}.

Spinor condensates have over the last few years been realized in both magnetic and optical traps. The latter are more interesting from the point of view of spin ordering, since the spin degree of freedom is not frozen out. The most widely studied atomic systems are those of the spin-1 alkali atoms ^{23}Na and ^{87}Rb . These systems differ from each other in the nature of the effective two-body interaction, which is antiferromagnetic in the former and ferromagnetic in the latter. The condensates with antiferromagnetic interactions are also called polar. Recent advances have made it possible to image ferromagnetic domains in optical traps of ^{87}Rb , making it possible to study the interesting physics of domain forma-

tion in them³. This technique requires the application of a magnetic field, an additional tunable parameter which makes the phase diagram of these systems interesting. Moreover, these atoms have also been trapped in two dimensional geometries, where the physics of collective behavior is often more exotic than in higher dimensions^{3,4}. The importance of this experiment for basic condensed matter physics is twofold: it probes both our understanding of phase-ordering kinetics at finite temperature (when observed at the longest times) and, as the temperature is lowered or the observation time is shortened, our understanding of dynamics across quantum phase transitions.

In this paper we will investigate magnetic domain formation in spin-1 systems at finite temperature and magnetic field. The main purpose of this study is to compare and contrast various plausible dynamical models with respect to coarsening of a magnetic order parameter. The quantity of primary interest, will be the dynamic critical exponent z which determines the rate of domain formation at large times: the domain size L grows with time as $L \sim t^z$. We will examine the general phase diagram of spin-1 condensates in the presence of a magnetic field in an optical trap and comment on the broken symmetries of the various ordered phases. We will then choose the phase that is most convenient to a study of magnetic domain formation and elucidate the similarities and differences between dynamic models, highlighting the importance of different conservation laws in the dynamics. We will compare our results with existing ones wherever possible.

A natural question is how the stochastic time-dependent Ginzburg-Landau (TDGL) approach in this paper is related to previous studies using deterministic equations of motion, such as the Gross-Pitaevskii equa-

tion for the condensate, plus quantum kinetic theory for excited states^{8,10,11}. The answer is that the correct description depends on experimental parameters such as the time scale of observation and the normal-state population. The time scale at which stochastic processes resulting from interaction with the normal cloud become important can be increased by decreasing the temperature of the system. The initial instability in a finite trap is likely to be described correctly by the deterministic theories in the literature; coupling to the many degrees of freedom in the normal cloud is irrelevant for the immediate dynamics of the condensate. However, the longer times accessed in current and future experiments are expected to be described by the theory developed here. In other words, the universal dynamical properties in the sense of critical phenomena are described by the theories presented here at any finite temperature, as long as the system is observed for a sufficiently long time. We believe that current experiments may already be in the regime where the theory presented here is valid. However, even if they are not, increases in observation time will soon enable a precise comparison between theory and experiment.

Our main results on phase ordering of spinor condensates are contained in sections VII and VIII. We argue in the final discussion that one specific dynamical model (“model F” dynamics, in the notation of the review paper of Hohenberg and Halperin¹²) is expected to describe the long-time dynamics of spinor condensates. This dynamical model is a more complicated version of the model used in earlier studies of superfluids^{13,14,15,16}, and reproduces the known propagating modes of the spinor condensate at zero temperature. All parameters in the dynamical model can be determined from measurements of the condensate, as explained in the appendix.

II. THE MAGNETIC PHASE DIAGRAM OF SPIN-1 BOSONS IN AN OPTICAL TRAP

Spin-1 condensates are theoretically more complex than those with zero spin^{5,17} in that the condensate order parameter is a three component complex vector

$$\Psi = \begin{pmatrix} \psi_{+1} \\ \psi_0 \\ \psi_{-1} \end{pmatrix}, \quad (1)$$

with ψ_α being the order parameter in the spin state of eigenvalue α along some arbitrarily chosen direction. If one assumes that the condensate state is a single particle zero momentum state, the total energy for a given density of atoms in an optical trap with a magnetic field B in the z direction can be written as

$$E = c_2 \langle \vec{S} \rangle^2 + g_2 \langle S_z^2 \rangle. \quad (2)$$

Here $\vec{S} = S_x \hat{x} + S_y \hat{y} + S_z \hat{z}$, where

$$\begin{aligned} S_x &= \frac{1}{\sqrt{2}} \begin{pmatrix} 0 & 1 & 0 \\ 1 & 0 & 1 \\ 0 & 1 & 0 \end{pmatrix} \\ S_y &= \frac{i}{\sqrt{2}} \begin{pmatrix} 0 & -1 & 0 \\ 1 & 0 & -1 \\ 0 & 1 & 0 \end{pmatrix} \\ S_z &= \begin{pmatrix} 1 & 0 & 0 \\ 0 & 0 & 0 \\ 0 & 0 & -1 \end{pmatrix} \end{aligned} \quad (3)$$

are the generators of $SU(2)$ in the spin-1 representation and $\langle A \rangle = \Psi^\dagger A \Psi$. c_2 is the spin-spin interaction which can be antiferromagnetic ($c_2 > 0$) or ferromagnetic ($c_2 < 0$). $g_2 \propto B^2$ and the second term is just the quadratic Zeeman term. The absence of a linear term is due to the fact that the time for the relaxation of magnetization in optical traps is less than the lifetime of the condensate itself. The ground state manifolds can be obtained by minimizing the free energy with respect to $\{\psi_\alpha^*\}$. It has already been shown that in the absence of a magnetic field, the ground state manifolds in the polar and ferromagnetic cases are isomorphic to the spaces $\frac{U(1) \times S^2}{Z_2}$ and $SO(3)$ respectively⁹. The phase diagram in the presence of a magnetic field is given below.

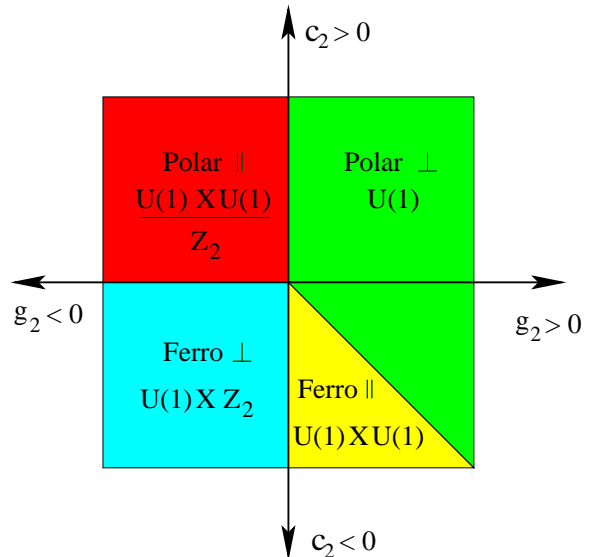


FIG. 1: The ground state phase diagram of a spin-1 condensate in an optical trap in the presence of a magnetic field that couples through a quadratic Zeeman term. The different quadrants have different phases with various types of in-plane and out-of-plane ordering. This figure has been taken from Mukerjee *et. al.*⁹.

Fig. 1 has four quadrants labelled by signs of c_2 and g_2 . In the polar ($c_2 > 0$) case, the magnetic ordering is either in plane or out of plane depending on the sign of g_2 . “Magnetic ordering” here refers to the ordering of the

spin-quantization axis ($\hat{\mathbf{n}}$). The ground state is always a macroscopically occupied single particle state of zero spin projection in this case. For $g_2 > 0$, the only symmetry that is broken in the ordered state is that of the $U(1)$ phase (θ) of the condensate. For $g_2 < 0$, however there is an additional $U(1)$ due to the in-plane ordering of the spin-quantization axis. The phase and spin are coupled through a Z_2 identification, which denotes symmetry under $\theta \rightarrow \theta + \pi$ and $\hat{\mathbf{n}} \rightarrow -\hat{\mathbf{n}}$. The vortices corresponding to the spin and phase are thus coupled and can lead to interesting finite-temperature physics in two dimensions¹⁸.

The lower part of the phase diagram corresponds to the ferromagnetic case ($g_2 < 0$) and will be of primary interest to us. The lower left quadrant corresponds to the case $g_2 < 0$. The ground state now breaks a $U(1)$ symmetry corresponding to the phase and an Ising Z_2 symmetry corresponding to the spin. Physically this means that in the condensate, the bosons are either in a state of spin projection 1 or -1. It is this Ising degree of freedom, we exploit to study domain formation in two dimensions. The reason is that since long range Ising order is possible in two dimensions (as opposed to $U(1)$ order), it is easier to define and measure the sizes of large magnetic domains required to investigate long time behavior. It is thus this quadrant that will be the focus of the rest of our studies. For the sake of completeness we note that the lower right quadrant, which corresponds to the case $g_2 > 0$ is divided into two parts by a straight line with equation $g_2 = 2c_2$. To the left of this line, one has in-plane ferromagnetic ordering with the spins pointing in some $U(1)$ direction in the plane. The ground state thus breaks two $U(1)$ symmetries, one corresponding to the phase and the other corresponding to the spin. To the right of the line, it is energetically favorable for the system to be in a polar out of plane state. This suggests the interesting possibility of a quantum phase transition in these systems tuned by the magnetic field.

III. 2D FINITE TEMPERATURE PHASE TRANSITIONS

Since we are interested in studying finite temperature coarsening dynamics in the 2D system with $c_2 < 0$ and $g_2 < 0$, it is important for us to locate the position of the superfluid and magnetic transitions. This problem is also interesting in its own right since such situations also come up in the study of classical frustrated spin systems, like the fully frustrated XY antiferromagnet (with π flux per plaquette) on a square lattice or the triangular lattice XY antiferromagnet, where the Z_2 corresponds to a chirality. The $U(1)$ and Z_2 transitions are in close proximity to each other in these cases. The situation is our particular case is not very different. We find that the $U(1)$ transition is of the Kosterlitz-Thouless (KT) type and the Z_2 transition of the 2D Ising type. Furthermore, we find that for a certain range of parameters, $T_{Z_2} > T_{U(1)}$ which is also what is observed in the fully frustrated XY model on the square lattice¹⁹ and for others the order of the transitions appears to be reversed. This depends on the magnitude of the ratio of the parameters g_2/c_2 . For small values of this ratio, $T_{Z_2} > T_{U(1)}$. There is presumably also a point where the two transitions occur at exactly the same temperature, where the combined transition is in a different universality class from 2D Ising and KT. We present here numerical data on just one set of parameters where $T_{Z_2} > T_{KT}$ and illustrate how the two transitions can be accurately determined despite being reasonably close to each other in temperature. The method used is due to Olsson¹⁹ and we employ a numerical Monte-Carlo simulations that uses the following Ginzburg-Landau free energy functional

$$F = \int d\mathbf{r} \left[\alpha \nabla \psi_a^* \nabla \psi_a + a_0 (T - T_c^{MF}) \psi_a^* \psi_a + \frac{c_0}{2} \psi_a^* \psi_b^* \psi_b \psi_a + \frac{c_2}{2} \psi_a^* \psi_a^* \mathbf{S}_{ab} \cdot \mathbf{S}_{a'b'} \psi_{b'} \psi_b + g_2 \psi_a^* (S_z^2)_{ab} \psi_b \right]. \quad (4)$$

with the following set of parameters, $\{\alpha = 0.5, a_0 = 5.5, c_0 = 7.0, c_2 = -2.4, g_2 = -1.3\}$.

The Kosterlitz-Thouless (KT) transition is detected by observing the temperature dependence of the helicity modulus Y . The helicity modulus for a discrete system of N lattice points is defined as

$$\Gamma = \frac{1}{N} \frac{\partial^2 \langle F \rangle}{\partial \delta^2} \Big|_{\delta=0} \quad (5)$$

where δ is a flux twist applied along a particular direction. The helicity modulus undergoes a jump of magnitude $\frac{2T_c}{\pi}$ at the location of the transition. This is shown in Fig. 2, where the transition temperature is seen to be $T_c \approx 0.44$.

The standard method to determine the location of the Z_2 transition using fourth order cumulants of the magnetic order parameter fails here for the same reason that it does in the case of the fully frustrated XY model, which is the proximity to the KT transition¹⁹. The cu-

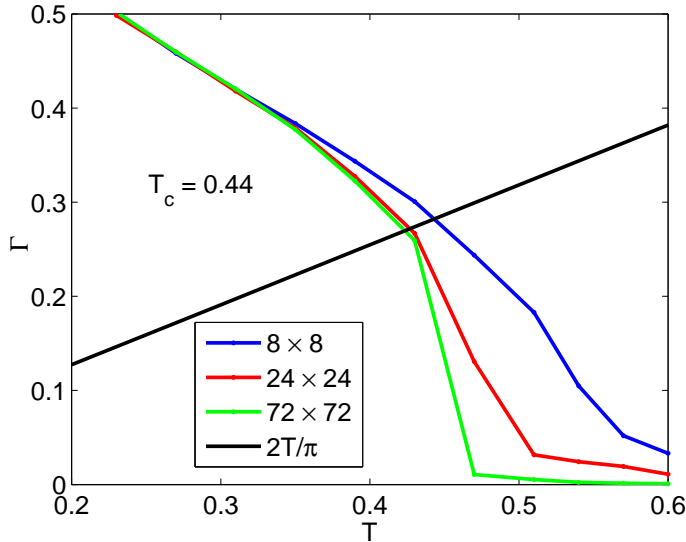


FIG. 2: The helicity modulus as function of Γ for the parameter set $\{\}$ for different system sizes. A clear jump is visible of $2T_c/\pi$ is visible at $T_c \approx 0.44$.

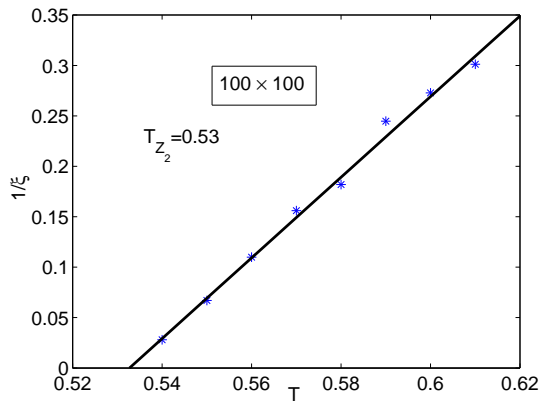


FIG. 3: The magnetic correlation length as a function of temperature fitted to the 2D Ising form. $T_c \approx 0.53$ as estimated this way.

mulant method assumes that the only relevant length scale at the transition is the system size which is not true here because of the large correlation length corresponding to the closely situated KT transition. Thus, a more accurate method is to look at the critical exponent of the correlation length of the magnetic order parameter

and determine T_c by fitting it to the expected 2D Ising form. The magnetization $M(\mathbf{r})$ is given by

$$M(\mathbf{r}) = |\psi_{+1}(\mathbf{r})|^2 - |\psi_{-1}(\mathbf{r})|^2. \quad (6)$$

The correlation length $\xi(T)$ can be extracted from the magnetic autocorrelation function

$$g(r) = \langle M(\mathbf{r})M(0) \rangle = e^{-r/\xi(T)}. \quad (7)$$

If the transition is 2D Ising like,

$$\xi(T) \sim \frac{1}{T - T_c}. \quad (8)$$

The numerical result is shown in Fig. 3, which shows that the correlation length fits the 2D Ising form fairly well. The obtained transition temperature is $T_c \approx 0.53$. A more careful finite-size scaling analysis can be done to determine the two transition temperatures, but even at this level of analysis it is clear that $T_{Z_2} > T_{U(1)}$.

IV. DYNAMICAL MODELS

The study of the formation of domains of the order parameter requires careful consideration of the dynamical modes of the system. Dynamical models are often constrained by conservation laws that are present as a consequence of symmetries or otherwise in the system. It is well known that the presence of conservation laws usually affects the rate of formation of domains, since the phase space of states that the system can pass through in the approach to the ordered state is constrained by the conservation laws. However, not all conservation laws affect domain formation in the same way and some might be more important than others. In this section we consider some dynamical models appropriate for the description of our system and comment on the conservation laws and the dynamical modes obtained from them.

The most commonly used dynamical model to describe spinor condensates is the Gross-Pitaevskii (GP) equation¹⁷. This is the model that has been extensively used to study domain formation in these systems. The model consists of treating the condensate as a classical field at zero temperature whose dynamics are given by the Hamilton equations of motion of the appropriate Hamiltonian. In our case, the Hamiltonian is

$$H = \int d\mathbf{r} \left[\frac{\hbar^2}{2m} \nabla \psi_a^* \nabla \psi_a + U(\mathbf{r}) \psi_a^* \psi_a + \frac{c_0}{2} \psi_a^* \psi_b^* \psi_b \psi_a + \frac{c_2}{2} \psi_a^* \psi_a^* \mathbf{S}_{ab} \cdot \mathbf{S}_{a'b'} \psi_{b'} \psi_b + g_2 \psi_a^* (S_z^2)_{ab} \psi_b \right], \quad (9)$$

with the dynamical equation of motion

$$i\hbar\frac{\partial\psi_a}{\partial t} = -\frac{\delta H}{\delta\psi_a^*} \quad (10)$$

It should be noted that the condensate density $\psi_a^*\psi_a$ and magnetization are both conserved by this equation. However, the GP equation cannot correctly describe the approach to equilibrium at finite temperatures, since the dynamics is only precessional and not relaxational. While this equation might be appropriate for the description of the dynamics once the condensate has been formed, it is inappropriate for the study of dynamic phenomena in other cases, for example quenches from high temperature where the energy of the condensate is not conserved.

The effect of finite temperature on the dynamics in spinor systems has thus far been taken into account through phenomenological rate equations, which too do not describe the approach to equilibrium. A simple model which is more appropriate is the so-called “model A” of the Hohenberg and Halperin classification¹². This model uses the Ginzburg-Landau free energy Eqn. 4 with simple Langevin dynamics. Operationally, this means the dynamical equation

$$\frac{\partial\psi_a}{\partial t} = -\Gamma_0\frac{\delta F}{\delta\psi_a^*} + \zeta_a(\mathbf{r}, t). \quad (11)$$

Thermal fluctuations due to finite temperature are contained in the noise variable $\zeta_a(\mathbf{r}, t)$, which has the following autocorrelation function

$$\langle\zeta_a^*(\mathbf{r}, t)\zeta_b(\mathbf{r}', t')\rangle = 2\text{Re}(\Gamma_0)k_B T\delta(\mathbf{r}-\mathbf{r}')\delta(t-t')\delta_{ab} \quad (12)$$

consistent with the fluctuation-dissipation theorem, that drives the system to equilibrium from a non-equilibrium state. This model like the GP model only considers the condensate as a classical field but unlike the GP model does not possess any conservation laws. It is relaxational in nature with the rate of relaxation of the order parameter set by $\text{Re } \Gamma_0$ and can be a complex number. The condensate density is no longer conserved and neither is the magnetization. The condensate is exchanging particles and energy with the “normal fluid” in this model. The non-conservation of energy of this model can be rectified by implicitly including the normal fluid through a conserved “second sound” mode (m), which is a real scalar field. Based on previous experience with the superfluid transition in helium, one expects that a correct description of the dynamics near the transition requires this additional field and in the notation of Hohenberg and Halperin, this model “model F”, with random forces ζ_a and θ for the fields ψ_a and m respectively. The free energy F_{SS} with this second-sound mode is

$$F_{\text{SS}} = F + \int d\mathbf{r} \left(\gamma_0 m \psi_a^* \psi_a + \frac{1}{2C_0} m^2 \right), \quad (13)$$

where F is given by Eqn. 4. The dynamics are given by

$$\begin{aligned} \frac{\partial\psi}{\partial t} &= -\Gamma_0\frac{\delta F_{\text{SS}}}{\delta\psi_a^*} - ig_0\psi\frac{\delta F_{\text{SS}}}{\delta m} + \zeta_a(\mathbf{r}, t) \\ \frac{\partial m}{\partial t} &= \lambda_0^m\nabla^2\frac{\delta F_{\text{SS}}}{\delta m} + 2g_0\text{Im}\left(\psi_a^*\frac{\delta F_{\text{SS}}}{\delta\psi_a^*}\right) + \tau(\mathbf{r}, t) \end{aligned} \quad (14)$$

These equations conserve the second sound density m and the noise correlator for θ , consistent with the fluctuation-dissipation theorem is

$$\langle\tau(\mathbf{r}, t)\tau(\mathbf{r}', t')\rangle = -2\lambda_0^m\nabla^2\delta(\mathbf{r}-\mathbf{r}')\delta(t-t') \quad (15)$$

The free energy F_{SS} has extra terms compared to F ; a term that couples m and the condensate density and others that contain the energy of the mode m . The dynamical equations also including coupling terms as a consequence of the non-vanishing Poisson brackets $\{m, \psi_a\}$ ^{20,21,22}. Aside from terms that result from derivatives of the Ginzburg-Landau free energy, there could in principle be additional magnetic terms analogous to those in the Heisenberg ferromagnet (e.g., $\mathbf{S}\times\nabla^2\mathbf{S}$, where \mathbf{S} is the local spin density). Since this is even in \mathbf{S} , it will not be obtained as the S derivative of any free energy, but will originate in the microscopic Hamiltonian. A check that no such additional terms are necessary is that the above equations reproduce the previously obtained modes in the GP equation. Such a calculation was carried out by Hohenberg and Halperin for the case of Helium and we extend that to the case of spinor condensates in the next section.

The three different dynamical models, GP, model A and model F are the ones we will use to investigate domain formation in spinor condensates at finite temperature and magnetic fields. We will in addition to the dynamical equations above also impose the conservation of magnetization on models A and F, to investigate the effect of that conservation law on the dynamics. As can be seen from the above discussion, model F contains many more parameters than model A and the GP equation. The parameters of this model are related to possible experimentally-measurable quantities in the appendix.

V. DYNAMICAL MODES IN THE ORDERED STATE

Model F contains in it both the GP equation and model A, which can be seen by setting the appropriate parameters in it to zero. However, it is important that model F produces all the dynamical modes that the GP equation does even when these parameters are not zero, in order for this treatment to be valid. There will also be additional modes produced (for example in m), that are absent in the GP equation. We explicitly demonstrate this in this section.

We begin by setting the temperature and magnetic field to zero, to enable comparison with the GP equation. The idea is to check that the introduction of the extra parameters of model F does not alter the modes that have already been calculated⁵. It is known that there are three linearly dispersing mode in the polar case and one gapped, linear and quadratic mode each in the ferromagnetic case. The dynamical equations describing the modes (either propagating or diffusion) are

$$\begin{aligned}\frac{\partial\psi_\alpha}{\partial t} &= -\Gamma_0\frac{\delta F_{SS}}{\delta\psi_\alpha^*} - ig_0\psi\frac{\delta F_{SS}}{\delta\psi_m} \\ \frac{\partial m}{\partial t} &= \lambda_0^m\nabla^2\frac{\partial F_{SS}}{\partial m} + 2g_0\text{Im}(\psi_\alpha^*\frac{\delta F_{SS}}{\delta\psi_\alpha^*})\end{aligned}\quad (16)$$

For brevity of notation, we also set $T = -a\nabla^2$, $\mu = a_0T_c^{MF}$ and explicitly write $\Gamma_0 = \Gamma_1 + i\Gamma_2$, where both Γ_1 and Γ_2 are real.

A. The polar case

We assume that

$$\Psi = N + \Phi, \quad (17)$$

where

$$N = \sqrt{n_0} \begin{pmatrix} 0 \\ 1 \\ 0 \end{pmatrix}, \quad (18)$$

is the value of the order parameter in the ordered polar state and Φ is a perturbation on it. The number of particles within the condensate, is related to the value μ and c_0 by minimizing the free energy F_{SS}

$$\sqrt{n_0} = \sqrt{\frac{\mu}{c_0}} \quad (19)$$

1. Polar state with $\Gamma_1 = 0$, $\lambda_0 = 0$, $\gamma = 0$

Let us first ignore the coupling $\gamma m\psi_\alpha^*\psi_\alpha$, as well as all the dissipation terms in the equations, like the term with coefficient Γ_1 and λ_0 . We will put them back in later.

In this case, all the modes are propagating, since there is no dissipation. After expanding the equations around N , the linearized equations we have are

$$\begin{aligned}\frac{\partial\phi_0}{\partial t} &= i\Gamma_2(T\phi_0 + 2c_0n_0(\phi_0 + \phi_0^*)) + im\frac{\sqrt{n_0}}{C}g_0 \\ \frac{\partial m}{\partial t} &= -ig_0\sqrt{n_0}\nabla^2(\phi_0 - \phi_0^*) \\ \frac{\partial\phi_1}{\partial t} &= -i\Gamma_2(T\phi_1 + n_0c_2(\phi_1 + \phi_{-1}^*)) \\ \frac{\partial\phi_{-1}}{\partial t} &= -i\Gamma_2(T\phi_{-1} + n_0c_2(\phi_{-1}^* + \phi_1))\end{aligned}\quad (20)$$

Notice that in order to get these equations, we need μ to take exactly the value in (19))

The equations for ϕ_1 and ϕ_{-1} have the same form as for the GP equation⁵, so the spin wave modes are the same. Both $M_+ = \phi_{+1} + i\phi_{-1}$ and $M_- = \phi_{+1} - i\phi_{-1}$ disperse linearly with k , with velocity $c_M = \Gamma_2\sqrt{n_0c_2}$.

The step by step solution for the coupled equation between ϕ_0 , ϕ_0^* and m is tedious, so we only write down the result here. Basically, the second sound mode and density fluctuation $\delta n_0 = \phi_0^* + \phi_0$ couple and form two modes with linear dispersion relations, the velocity is

$$c_s = \sqrt{\frac{g_0^2n_0}{C} + 2a\Gamma_2^2c_0n_0} \quad (21)$$

Notice that the first term in the square root in the above equation is the square of the second sound velocity¹², with $\Gamma_2 = 0$ and ignoring the propagating mode of ψ . The second term in the square root is the one that appears as the density fluctuation mode in Ref. 5, where the the second sound mode was ignored. Here we see that if we take into account both densities, the second sound mode and the density fluctuation mode couple into a new mode with velocity c_s .

2. Polar state with $\Gamma_1 = 0$, $\lambda_0 \neq 0$, $\gamma = 0$

Here the dissipation λ_0 term is added back into the equations. We will not consider the case with finite Γ_1 , since we assume that within the condensate, the dissipation of the modes is very small.

The coupled equations between m and ϕ_0 now become

$$\begin{aligned}\frac{\partial\phi_0}{\partial t} &= i\Gamma_2(T\phi_0 + 2c_0n_0(\phi_0 + \phi_0^*)) + im\frac{\sqrt{n_0}}{C}g_0 \\ \frac{\partial m}{\partial t} &= -ig_0\sqrt{n_0}\nabla^2(\phi_0 - \phi_0^*) + \frac{\lambda_0}{C}\nabla^2m\end{aligned}\quad (23)$$

The detailed solution is again tedious and we will solve the equation based on following approximation that the higher order terms of spatial derivatives are small, since we are only interested in the limit k going to zero. Under this approximation the dispersion relation is

$$\omega = c_s k + i\frac{\lambda_0}{C}k^2 \quad (24)$$

The mode gets a propagating part, which is linear in k , and a damping part, which is proportional to k^2 . c_s is given by (21).

3. *Polar state with $\Gamma_1 = 0$, $\lambda_0 \neq 0$, $\gamma \neq 0$*

Turning on γ , changes only two terms in the equations. First,

$$\frac{\partial \phi_0}{\partial t} = i\Gamma_2(T\phi_0 + 2c_0n_0(\phi_0 + \phi_0^*)) + ig_0\gamma n_0(\phi_0 + \phi_0^*) + im\frac{\sqrt{n_0}}{C}g_0. \quad (25)$$

We can redefine

$$c'_0 = c_0 + \frac{g_0\gamma}{\Gamma_2} \quad (26)$$

and make the equation look exactly like (20), except for replacing c_0 by c'_0 . γ also modifies (23), by adding a term to the right hand side

$$\begin{aligned} \frac{\partial \phi_0}{\partial t} &= i\Gamma_2(T\phi_0 + 2c_0n_0(\phi_0 + \phi_0^*)) + im\frac{\sqrt{n_0}}{C}g_0 \\ \frac{\partial m}{\partial t} &= -ig_0\sqrt{n_0}\nabla^2(\phi_0 - \phi_0^*) + \frac{\lambda_0}{C}\nabla^2m \\ &\quad + \frac{\lambda_0\gamma}{C}\sqrt{n_0}\nabla^2(\phi_0 + \phi_0^*) \end{aligned} \quad (27)$$

Solving this modified equation, we see that the term proportional to γ only contributes higher order momentum terms. So, up to linear order in k , the dispersion relation is not changed. Therefore all the results here are the same as case 2, if we replace c_0 by c'_0 .

B. The ferromagnetic case

The solution of the ferromagnetic case is very similar to the polar case. The general formalism and effective action Eqn. 13 still apply. The difference is in how we linearize the equations. In the ferromagnetic case, we should linearize the equations around the state

$$\Psi = N + \Phi, \quad (28)$$

with

$$N = \sqrt{n_0} \begin{pmatrix} 1 \\ 0 \\ 0 \end{pmatrix} \quad (29)$$

Here the density of the condensate is not only related to the coefficient c_0 , but also to the coefficient c_2 .

$$\sqrt{n_0} = \sqrt{\frac{\mu}{c_0 + c_2}} \quad (30)$$

We now obtain the following linearized equations

$$\begin{aligned} \frac{\partial \phi_1}{\partial t} &= i\Gamma_2(T\phi_0 + 2(c_0 + c_2)n_0(\phi_1 + \phi_1^*)) + im\frac{\sqrt{n_0}}{C}g_0 \\ \frac{\partial m}{\partial t} &= -ig_0\sqrt{n_0}\nabla^2(\phi_1 - \phi_1^*) + \frac{\lambda_0}{C}\nabla^2m \end{aligned}$$

$$\begin{aligned} \frac{\partial \phi_0}{\partial t} &= -i\Gamma_2T\phi_0 \\ \frac{\partial \phi_{-1}}{\partial t} &= -i\Gamma_2T\phi_{-1} + 2c_2n_0\phi_{-1} \end{aligned} \quad (31)$$

The dispersion relation for the second sound mode is

$$\begin{aligned} \omega &= c_s k + i\frac{\lambda_0}{C}k^2 \\ c_s &= \sqrt{\frac{g_0^2 n_0}{C} + 2a\Gamma_2^2(c_0 + c_2)n_0}, \end{aligned} \quad (32)$$

where we have kept terms only to lowest order in the momentum in every step of the calculation. For the density fluctuation mode $\delta n = \sqrt{n_0}(\phi_1 + \phi_1^*)$, the dispersion relation is

$$\omega = c_s k \quad (33)$$

The spin wave mode $\delta M_- = \sqrt{n_0}\phi_0^*$ has the same dispersion relation as the one obtained in the GP case⁵, $\omega = ak^2$. Again, turning on the interaction γ does not change the result much. It causes a redefinition of c_0 in the propagating part of the mode, and only contributes higher order momentum terms in the diffusion or damping part of the mode, which are not important when the momentum is small.

Thus, we see that in both the polar and ferromagnetic cases, the dynamic modes obtained in the presence of the extra parameters of model F are consistent with those obtained from the GP equations. The nature of the density mode changes because of coupling with the second sound mode but the spin wave modes remain unaffected.

VI. DOMAIN FORMATION

A typical experiment or numerical simulation of coarsening involves starting the system off at a high-temperature (usually disordered) state and rapidly quenching it to a temperature below the ordering transition to observe the growth of domains of the ordered state. At the heart of the theoretical analysis of this process is the scaling hypothesis²³. The equal-time correlation function of the order parameter $m(\mathbf{r}, t)$ is defined as

$$C(\mathbf{r}, t) = \langle m(\mathbf{x} + \mathbf{r}, t)m(\mathbf{r}, t) \rangle. \quad (34)$$

The scaling hypothesis states that

$$C(\mathbf{r}, t) = f\left(\frac{r}{L(t)}\right) \quad (35)$$

$L(t)$ is a characteristic length scale, the domain size. Further, at long times $L \propto t^{1/z}$, where z , the dynamical critical exponent. The dynamical critical exponent is

dependent on the model used to describe the ordering dynamics of the system, the symmetry of the order parameter and the nature of defects present in the initial state. For instance, it is known that $z = 2$ for the Ising model with dynamics which do not conserve the total magnetization, after a high temperature quench. For an XY model on the other hand $z = 2$ but with a logarithmic correction as a function of time²³. The difference from the Ising case can be attributed to the different broken symmetry and consequently the topological defects present in the high temperature state. The Ising model with a conserved order parameter on the other hand produces a different dynamic critical exponent $z = 3$ ^{23,24}. The growth of domains is slower in this case compared to the case with no magnetization conservation since the conservation law places constraints on the phase space available during domain growth.

VII. DETAILS OF THE NUMERICAL SIMULATION

In this work we study the dynamics of domain growth in 2D after a magnetic field quench and not a temperature quench. The motivation is a similar approach adopted in recent experiments in optical traps. To be specific, we study a ferromagnetic condensate in two dimensions whose initial state is a polar out-of-plane state in the fourth quadrant of Fig. 1 and quench it to a value of the field, where the ordered state is a ferromagnetic out-of-plane state (in quadrant 3 of Fig. 1). Operationally, we sweep the parameter g_2 from a large positive value to a negative value. For models A and F, this is done at finite temperature and the order parameter eventually relaxes to a uniform value consistent with the ferromagnetic out-of-plane state. The Gross-Pitaevskii equation on the other hand does not cause the system to relax but rather to oscillate between different concentrations of the three spinor components. Further, it does not allow an initial state which is completely polar out-of-plane to form magnetic domains of the +1 and -1 components at any value of the time. In this case, we start with an initial state, which has 90% of the atoms in the 0 (polar out-of-plane) state and the other 10%, divided equally among the +1 and -1 states. The phase of each spinor component in the initial state is chosen to be a random number between 0 and 2π allowing for spatial inhomogeneity which leads to domain formation.

The equations of motion corresponding to each model are integrated numerically using a first order Euler method with the noise functions drawn from a Gaussian distribution. The size of the numerical grid ranges from 50×50 to 200×200 . The time step is adjusted depending on the values of the other parameters and varied to check for consistency. The number of parameters is large

(especially for model F) and we present results only for a fixed set of parameters. However, we have explored other parts of the parameter space consistent with ferromagnetic out-of-plane order and not found any qualitative and wherever appropriate (like for the value of z) quantitative difference in the results. The set of parameters for which we report results are those in section III with the additional model F parameters, $\{\text{Re}(\Gamma_0) = 1.30, \text{Im}(\Gamma_0) = 0.26, g_0 = 0.35, \lambda_0^m = 0.84, \gamma_0 = 1.5\}$, wherever applicable.

The domain size $L(t)$ is measured using the relation

$$L(t) = \sqrt{\frac{S_0(t)}{S_2(t)}}, \quad (36)$$

where $S_0(t)$ and $S_2(t)$ are respectively the zeroth and second moment of the structure function

$$S(\mathbf{k}, t) = \int d\mathbf{r} \langle M(\mathbf{r}, t) M(0, t) \rangle e^{i\mathbf{k} \cdot \mathbf{r}}, \quad (37)$$

which is the Fourier transform of the order parameter correlation function. The domain size is also calculated by measuring the size of domain boundaries directly in the simulation grid. This method serves as a consistency check on the first method. It should be mentioned though that the second method is useful and consistent with the first one only when there are very few small bubbles of one value of the order parameter inside large islands of the other value. This method essentially ignores these bubbles by looking for large closed domain walls and works best when the domains are large in size.

VIII. RESULTS

A. Finite temperature without conservation of magnetization

We present results for the domain size as a function of time for models A and F in Fig 4. The results presented are for the set of parameters mentioned in the preceding section, with a magnetic field quench and have been obtained on a grid of size 200×200 . It can be seen that domain formation is faster for model A than for model F, which can be attributed to the presence of the extra conservation law. This certainly appears to be the case over the range of parameters that we have explored, but may not be the case elsewhere in parameter space. Whether or not this is a universal feature requires more careful analysis. The curve for $L(t)$ as a function of t for model A dynamics seems to yield a $z = 2 \pm 0.15$ over the entire range of values of time we have presented. Further, the value of z obtained at different values of time seems to be fairly constant. This is the value of z , one would expect for a high temperature quench in a pure Ising model.

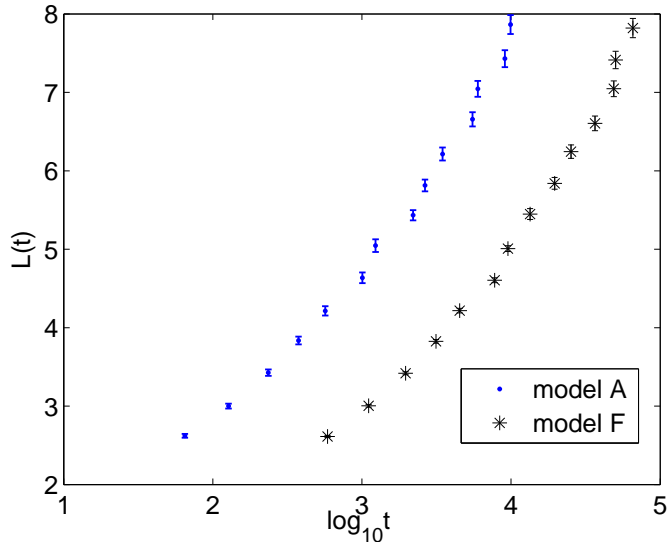


FIG. 4: $L(t)$ as a function of $\log_{10} t$ for model F with the parameter set \mathcal{R} , with no magnetization conservation .

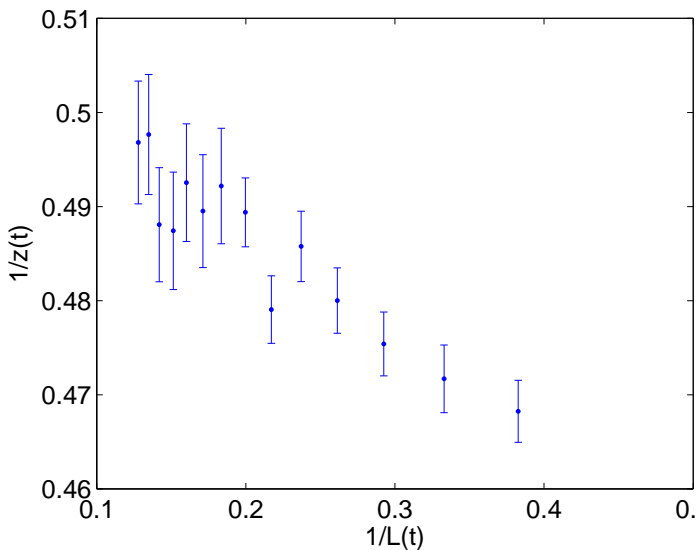


FIG. 5: $1/z(t)$ as a function of $1/L(t)$ for model F and no magnetization conservation with the parameter set \mathcal{R} demonstrating the drift of $z(t)$ as a function of t and thus increasing $L(t)$ towards the value $z = 2$.

Model F also yields $z \approx 2$. Unlike in model A dynamics, there is a small drift in the value of z obtained at different values of t . A similar drift (of a larger magnitude) has been seen in the case of the Ising model with dynamics that conserve magnetization and it has been argued by Huse²⁴ that this is due to excess transport in domain interfaces. It then follows that the effective dynamic critical exponent $z(t)$ drifts in the following way

to first order in the domain size

$$\frac{1}{z(t)} = \frac{1}{z(t = \infty)} \left[1 - \frac{L_0}{L(t)} \right] \quad (38)$$

This suggests that $z(t)$ approaches its infinite time value from above, which appears to be the case here as well as can be seen from Fig. 5 , which is a plot of $1/z(t)$ vs. $1/L(t)$. However, we emphasize that the above analysis is strictly applicable only to the case where the *order parameter is conserved*, which is not the case here. The quantity that is conserved is the second sound mode. Nevertheless, it is possible that the drift can be explained by some mechanism similar to the above.

To conclude this part, we remark that both models A and F without any explicit magnetization conservation both yield the same dynamic critical exponent $z = 2$ for coarsening with a magnetic field quench.

B. Finite temperature with conserved magnetization

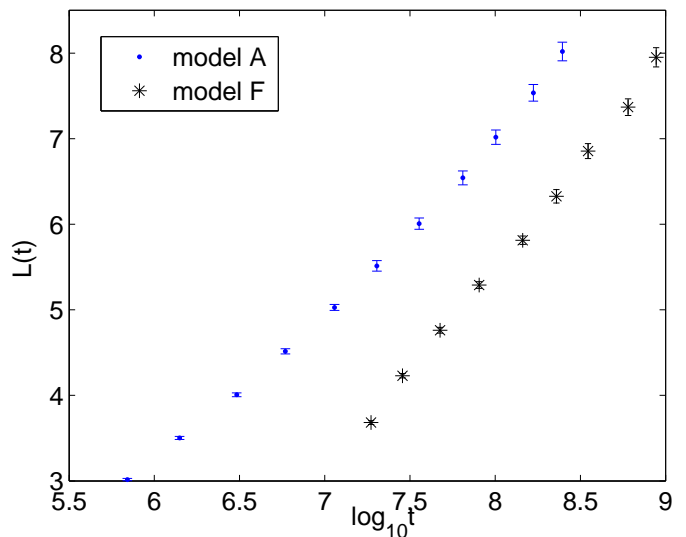


FIG. 6: $L(t)$ as a function of $\log_{10} t$ for models A and F and conserved magnetization density with the parameter set \mathcal{R} .

We now present results for models A and F with conserved magnetization. The magnetization conservation is implemented in terms of a local continuity equation in the magnetization density and a magnetization current. We illustrate how we do this for model A and the implementation for model F proceeds along similar lines. We first note that the magnetization density $M = |\psi_{+1}(\mathbf{r}, t)|^2 - |\psi_{-1}(\mathbf{r}, t)|^2$ only involves the amplitudes of the components of the condensate order parameter. We first write down model A dynamics in terms of

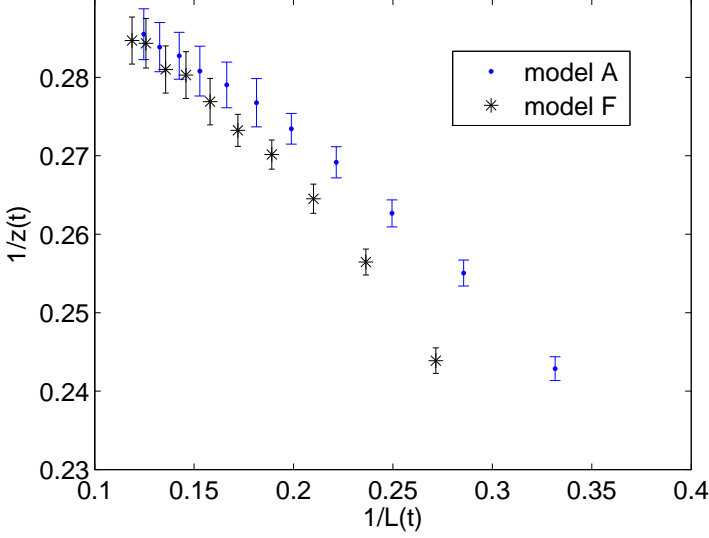


FIG. 7: $1/z(t)$ as a function of $1/L(t)$ for models A and F and conserved magnetization density with the parameter set \mathcal{R} demonstrating the drift of $z(t)$ as a function of t and thus increasing $L(t)$ towards the value $z = 3$.

separate dynamical equations for the phase and amplitude of each component of the condensate order parameter. These turn out to be

$$\frac{\partial|\psi_a|}{\partial t} = -\frac{1}{2}\text{Re}(\Gamma_0)\frac{\delta F}{\delta|\psi_a|} + \frac{1}{2|\psi_a|}\text{Im}(\Gamma_0)\frac{\delta F}{\delta\theta_a} + \mu_a(\mathbf{r}, t), \quad (39)$$

$$|\psi_a|\frac{\partial\theta_a}{\partial t} = -\frac{1}{2|\psi_a|}\text{Re}(\Gamma_0)\frac{\delta F}{\delta\theta_a} + \frac{1}{2}\text{Im}(\Gamma_0)\frac{\delta F}{\delta|\psi_a|} + \nu_a(\mathbf{r}, t), \quad (40)$$

where the noise correlators are

$$\begin{aligned} \langle\mu_a(\mathbf{r}, t)\mu_b(\mathbf{r}', t')\rangle &= \langle\nu_a(\mathbf{r}, t)\nu_b(\mathbf{r}', t')\rangle \\ &= \text{Re}(\Gamma_0)k_B T\delta(\mathbf{r}-\mathbf{r}')\delta(t-t')\delta_{ab}. \end{aligned} \quad (41)$$

Note that every quantity in the above equations is now real. If we were interested in conserving the density $|\psi_a|^2$ of each component *individually*, we would modify Eqn. 39 to

$$\begin{aligned} \frac{\partial|\psi_a|^2}{\partial t} &= -\text{Re}(\Gamma_0)\nabla^2\left(|\psi_a|\frac{\delta F}{\delta|\psi_a|}\right) + \text{Im}(\Gamma_0)\nabla^2\left(\frac{\delta F}{\delta\theta_a}\right) \\ &+ \mu_a(\mathbf{r}, t), \end{aligned} \quad (42)$$

with the correlator for μ now given by

$$\langle\mu_a(\mathbf{r}, t)\mu_a(\mathbf{r}', t')\rangle = 4\text{Re}(\Gamma_0)\nabla^2[|\psi_a(\mathbf{r}, t)|^2\delta(\mathbf{r}-\mathbf{r}')]\delta(t-t'). \quad (43)$$

This ensures there is a conservation equation of the sort

$$\frac{\partial|\psi_a(\mathbf{r}, t)|^2}{\partial t} = -\nabla\cdot\mathbf{J}_a(\mathbf{r}, t) \quad (44)$$

for each component. We are however not interested in conserving the density of each component, but only the combination $M = |\psi_{+1}|^2 - |\psi_{-1}|^2$. To this end, proceeding as above, we obtain the following set of equations.

$$\frac{\partial M}{\partial t} = -\text{Re}(\Gamma_0)\nabla^2\left(|\psi_{+1}|\frac{\delta F}{\delta|\psi_{+1}|} - |\psi_{-1}|\frac{\delta F}{\delta|\psi_{-1}|}\right) + \text{Im}(\Gamma_0)\nabla^2\left(\frac{\delta F}{\delta\theta_{+1}} - \frac{\delta F}{\delta\theta_{-1}}\right) + \mu_M(\mathbf{r}, t) \quad (45)$$

$$\frac{\partial N}{\partial t} = -\text{Re}(\Gamma_0)\left(|\psi_{+1}|\frac{\delta F}{\delta|\psi_{+1}|} + |\psi_{-1}|\frac{\delta F}{\delta|\psi_{-1}|}\right) + \text{Im}(\Gamma_0)\left(\frac{\delta F}{\delta\theta_{+1}} + \frac{\delta F}{\delta\theta_{-1}}\right) + \mu_N(\mathbf{r}, t) \quad (46)$$

$$\frac{\partial|\psi_0|}{\partial t} = -\frac{1}{2}\text{Re}(\Gamma_0)\frac{\delta F}{\delta|\psi_0|} + \frac{1}{2|\psi_0|}\text{Im}(\Gamma_0)\frac{\delta F}{\delta\theta_0} + \mu_0(\mathbf{r}, t) \quad (47)$$

$$|\psi_a|\frac{\partial\theta_a}{\partial t} = -\frac{1}{2|\psi_a|}\text{Re}(\Gamma_0)\frac{\delta F}{\delta\theta_a} + \frac{1}{2}\text{Im}(\Gamma_0)\frac{\delta F}{\delta|\psi_a|} + \nu_a(\mathbf{r}, t) \quad (48)$$

Here $N = |\psi_{+1}|^2 + |\psi_{-1}|^2$ and the noise correlators are given by

$$\begin{aligned} \langle\mu_M(\mathbf{r}, t)\mu_M(\mathbf{r}', t')\rangle &= 4\text{Re}(\Gamma_0)\nabla^2[\{|\psi_{+1}(\mathbf{r}, t)|^2 + |\psi_{-1}(\mathbf{r}, t)|^2\}\delta(\mathbf{r}-\mathbf{r}')]\delta(t-t') \\ \langle\mu_N(\mathbf{r}, t)\mu_N(\mathbf{r}', t')\rangle &= 4\text{Re}(\Gamma_0)\{|\psi_{+1}(\mathbf{r}, t)|^2 + |\psi_{-1}(\mathbf{r}, t)|^2\}\delta(\mathbf{r}-\mathbf{r}')\delta(t-t') \\ \langle\mu_0(\mathbf{r}, t)\mu_0(\mathbf{r}', t')\rangle &= \text{Re}(\Gamma_0)k_B T\delta(\mathbf{r}-\mathbf{r}')\delta(t-t') \\ \langle\nu_a(\mathbf{r}, t)\nu_b(\mathbf{r}', t')\rangle &= \text{Re}(\Gamma_0)k_B T\delta(\mathbf{r}-\mathbf{r}')\delta(t-t')\delta_{ab} \end{aligned} \quad (49)$$

The noise functions μ_N , μ_M , μ_0 and ν_a are mutually uncorrelated. The above equations for M and N can be

used to generate equations for $|\psi_{+1}|$ and $|\psi_{-1}|$, which is the way the numerical calculation is performed. Note that the full set of dynamical equations written above has no conservation law except the one for M . We now

use the same procedure to impose magnetization conservation on model F. The dynamical equations in this case are

$$\frac{\partial M}{\partial t} = -\text{Re}(\Gamma_0)\nabla^2 \left(|\psi_{+1}| \frac{\delta F_{ss}}{\delta |\psi_{+1}|} - |\psi_{-1}| \frac{\delta F_{ss}}{\delta |\psi_{-1}|} \right) + \text{Im}(\Gamma_0)\nabla^2 \left(\frac{\delta F_{ss}}{\delta \theta_{+1}} - \frac{\delta F_{ss}}{\delta \theta_{-1}} \right) + \mu_M(\mathbf{r}, t) \quad (50)$$

$$\frac{\partial N}{\partial t} = -\text{Re}(\Gamma_0) \left(|\psi_{+1}| \frac{\delta F_{ss}}{\delta |\psi_{+1}|} + |\psi_{-1}| \frac{\delta F_{ss}}{\delta |\psi_{-1}|} \right) + \text{Im}(\Gamma_0) \left(\frac{\delta F_{ss}}{\delta \theta_{+1}} + \frac{\delta F_{ss}}{\delta \theta_{-1}} \right) + \mu_N(\mathbf{r}, t) \quad (51)$$

$$\frac{\partial |\psi_0|}{\partial t} = -\frac{1}{2}\text{Re}(\Gamma_0) \frac{\delta F_{ss}}{\delta |\psi_0|} + \frac{1}{2|\psi_0|}\text{Im}(\Gamma_0) \frac{\delta F_{ss}}{\delta \theta_0} + \mu_0(\mathbf{r}, t) \quad (52)$$

$$|\psi_a| \frac{\partial \theta_a}{\partial t} = -\frac{1}{2|\psi_a|}\text{Re}(\Gamma_0) \frac{\delta F_{ss}}{\delta \theta_a} + \frac{1}{2}\text{Im}(\Gamma_0) \frac{\delta F_{ss}}{\delta |\psi_a|} - g_0 |\psi_a| \frac{\partial F_{ss}}{\partial m} + \nu_a(\mathbf{r}, t) \quad (53)$$

$$\frac{\partial m}{\partial t} = \lambda_0^m \nabla^2 \frac{\delta F_{SS}}{\delta m} + g_0 \text{Im} \left(|\psi_a| \frac{\delta F_{SS}}{\delta |\psi_a|} \right) + \tau(\mathbf{r}, t) \quad (54)$$

The noise correlators are the same as for model A with magnetization conservation with the additional correlator

$$\langle \tau(\mathbf{r}, t) \tau(\mathbf{r}', t') \rangle = -2\lambda_0^m \nabla^2 \delta(\mathbf{r} - \mathbf{r}') \delta(t - t'), \quad (55)$$

as in the case of model F without magnetization conservation. It should be noted that the coefficient g_0 appears only in the dynamical equation for the phases of the different components of the condensate thus making its identification as a precessional term obvious. Further, the above dynamical equations conserve both the magnetization M and the second sound mode m and thus represent perhaps the most realistic dynamical model for a BEC at finite temperature and field; one where the condensate can exchange charge and energy with the “normal cloud” but not magnetization.

Once again, the results presented are for a 200×200 simulation grid. We have checked that the additional magnetization conservation law does not affect the static properties of the model. As in the previous case, we again see that domain formation is faster for model A and than model F. This time, however, the dynamic critical exponent obtained is not equal to 2. As can be seen from Fig. 7, which is a plot of $1/z(t)$ vs. $1/L(t)$ for both models, there is a significant drift of $z(t)$ as a function of time. Once again the direction of the drift is consistent with Eqn. 38 and in this case, the analysis mentioned in the previous subsection is directly applicable, since it is the order parameter (the magnetization) that is directly conserved. However, the noise levels of the simulations do not permit a fit to Eq. 38. It should be noted though that to the extent observable in the numerical simulation, there is a drift in the direction of $z = 3$ in the data. This is what is observed in a pure Ising model with con-

served magnetization in a high temperature quench. One interesting observation is that the value of $1/z(t)$ seems to deviate more strongly from Eq. 38 at large times for model F than model A. This deviation has also been observed for the simple Ising model with conserved magnetization, where it was attributed to finite-size effects and correlated noise in the simulations. That could well be the case here as well, although it is not clear why these effects should be more pronounced in one model than in the other. It should be noted that in the simulations on the Ising model²⁴, the values of $z(t)$ observed for comparable simulation times are roughly close to what we observe.

The conclusion of this part is that models A and F with explicit magnetization conservation yield a dynamic critical exponent $z \approx 3$, different from the exponent obtained without magnetization conservation. Thus, the models A and F seem to be identical as far as long-time coarsening behavior of the magnetization is concerned and the behavior is truly determined by whether or not the magnetization is conserved, which it is not explicitly in either model. The difference between these two models will become apparent, when the coarsening of domains related to the conserved second mode is investigated.

C. The Gross-Pitaevskii equation

We finally investigate domain formation in the Gross-Pitaevskii equation. As has been remarked earlier, this formalism assumes that the dynamics of the condensate is completely determined by the precessional (and not re-

laxational) dynamics of the classical order parameter. It is thus a formalism that on the one hand is valid strictly at zero temperature, but on the other hand ignores quantum fluctuations. The initial state chosen for models A and F considered earlier does not evolve in this formalism and hence we choose a slightly different initial state as mentioned in section VII with 90% of the condensate density in the 0 state and 5% each in the +1 and -1 states. The precessional nature of the GP equation implies that there is never any true relaxation to a state with only domains of +1 and -1 and the amplitudes of these two components oscillate together, $\pi/2$ out of phase with the amplitude of the 0 component. The dynamical critical exponent z in these simulations is extracted by looking at the time interval when the amplitudes of the +1 and -1 components are growing with time and that of the 0 component falling. It is important that a sizeable window be identified within this interval where the domain size $L(t)$ is indeed growing as $L(t) \propto t^{1/z}$. The oscillatory nature of the dynamics ensures that in this case, both the magnetization and condensate density are conserved. The former is manifested in the fact the +1 and -1 components always have the same amplitude and the latter in the fact that these two components are always $\pi/2$ out of phase with the 0 component.

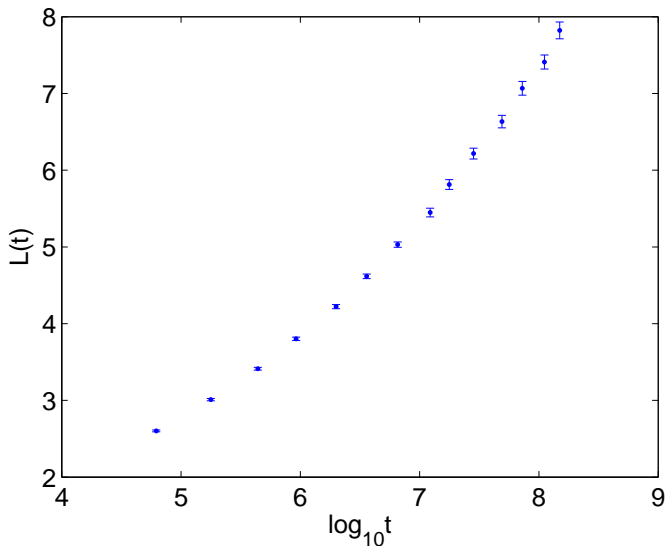


FIG. 8: $L(t)$ as a function of $\log_{10} t$ in the GP equation with the parameter set \mathcal{R} . The data is from a time interval during which the amplitudes of the ± 1 components are increasing with time.

The domain size here is obtained only using Eqn. 36 since the presence of bubbles of the 0 state renders the method of measuring the domain boundaries directly unreliable. The data for the domain size $L(t)$ as a function of t is shown in Fig. 8. The data as in the previous two cases has been obtained over a range of about four decades. The dynamic critical exponent $z(t)$ as extracted is shown as a function of $1/L(t)$. Once again, there ap-

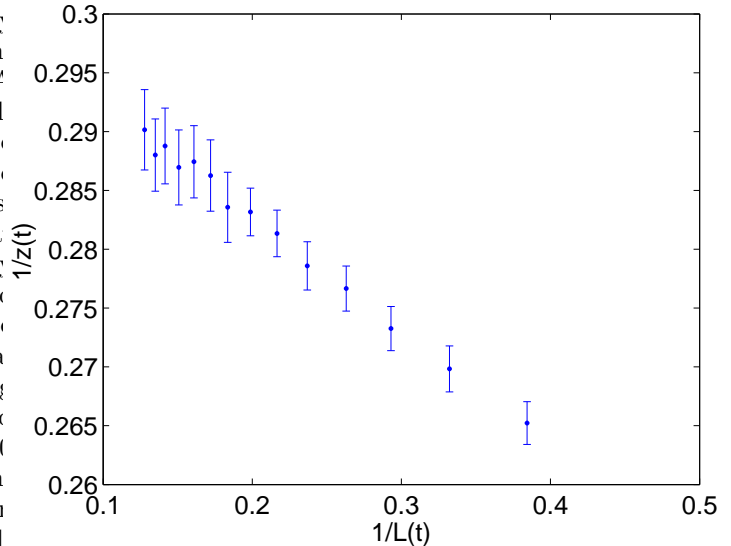


FIG. 9: $1/z(t)$ as a function of $1/L(t)$ in the GP equation with the parameter set \mathcal{R} . The exponent $z(t)$ as a function of t and thus increasing $L(t)$ seems to drift towards the value $z = 3$ like with models A and F with conserved magnetization densities.

pears to be a drift towards the value $z = 3$ at infinite time, although in this case, it appears (to within the noise) that the drift is more consistent with Eqn. 38 (i.e. linear in $1/L(t)$) than for models A and F .

It appears that the GP model gives a different dynamic critical exponent $z = 3$ from models A and F ($z = 2$), unless magnetization is conserved explicitly in the latter. This should be compared and contrasted with the case of spinless bosons, where it has been hypothesized that model F and the GP equation give the same dynamic critical exponent for phase ordering²⁵. Further, this exponent was numerically found to be equal to 1 (different from model A , which has $z = 2$) from numerical studies of the GP equation in this case. The situation we analyze is different from the case of spinless bosons in that we study the magnetization. The second sound mode of model F arises from total energy and number conservation between the condensate and the “normal state”. The GP equation too conserves both these quantities. However, for bosons with spin, the GP equation also conserves magnetization, which is not present in model F unless included by hand. Thus the value of z for the GP equation is different from that of model F and agreement is obtained only when magnetization is explicitly conserved in the latter. It is interesting to note however that the value of z obtained from the GP equation is larger than from model A in our study whereas for spinless bosons it is smaller.

IX. CONCLUSIONS

To conclude, we have studied the statics and dynamics of spin-1 condensates at finite temperature in the presence of a magnetic field. We have obtained a ground state phase diagram for this system and have focussed on the phase that is most amenable to a numerical study of magnetic domain formation in 2D, namely the Ferromagnetic out-of-plane phase and have numerically determined the nature and order of the superfluid and magnetic phase transitions. We have argued that the “correct” dynamical model for spinor condensates at finite field and temperature is model F in the Halperin and Hohenberg classification and have demonstrated that this model contains all the modes in the standard GP equation. We have numerically studied magnetic domain formation in the GP model and models A and F with and without magnetization conservation, and have found that it is the only when magnetization is explicitly conserved in models A and F that the dynamic critical exponent z obtained from the GP equations agrees with the z obtained from them. In the absence of this conservation, models A and F yield $z = 2$.

While we have focussed only on one part of the phase diagram of spinor condensates in this study to highlight the difference between various dynamical models, similar studies can be performed in the other parts of the phase diagram as well. This will be reported elsewhere. It is our belief that model F is fundamentally a more complete dynamical model to describe spinor condensates than the GP model. In addition to studies of the dynamics far away from the critical point, as presented here, this dynamical model could be used to obtain dynamical critical exponents, for comparison to dynamical experiments near the static phase transition of the spinor condensate.

APPENDIX A: RELATION OF THE MODEL F PARAMETERS TO MEASURABLE QUANTITIES

As remarked earlier, Model F has many more parameters than the GP equation. Here we comment on how these parameters can be related to experimentally measurable quantities. There are 9 important real parameters, which are Γ_1 , Γ_2 , g_0 , λ_0 , μ , c_0 , c_2 , C , γ . Some of them are directly measurable. For example, λ_0 is the thermal conductivity, and C is the specific heat. We now discuss how to measure all the other parameters.

1. g_0

g_0 only exists in the dynamical equations and does not appear in the static free energy. In the general formalism, at the operator level, it appears in the Poisson bracket between m and ψ_a as

$$[\psi_a^\dagger, m] = g_0 \psi_a^\dagger \quad (\text{A1})$$

This means if we create a particle through ψ_a^\dagger , the expectation value of m in the system increases by g_0 . Since m is effectively the “heat” in the system (this can be seen from the physical meaning of C and λ), g_0 is effectively the “heat” per particle. Writing,

$$g_0 = T\sigma, \quad (\text{A2})$$

where σ is the entropy per particle, the value of g_0 can now be obtained from measuring the specific heat

$$g_0 = T \int_0^T dT \frac{c}{T}. \quad (\text{A3})$$

Here c is the specific heat per particle.

2. $c_0 + C\gamma^2$

The reason we discuss c_0 and γ together is that c_0 and γ can only appear in the combination $c_0 + \gamma^2$ in all static quantities. This can be seen from mean field theory: m appears in a quadratic term $1/(2C)m^2$ and a linear term γmn_0 : the expectation value of m is thus $C\gamma$. Plugging this value of m into Eqn. 13, the m^4 interaction term becomes $c_0 + C\gamma^2$, which we denote as c' . How do we measure c' ? At low temperature, almost all the atoms are in the condensate. All the terms in Eqn. 13 are proportional to the density of the condensate, except the c' term which is proportional to the square of the density. This term will therefore contribute to the compressibility κ of the condensate, where

$$\kappa^{-1} = -V \frac{dP}{dV} = V \frac{d^2 E}{dV^2} = 2c'n_0^2 \quad (\text{A4})$$

When the temperature is low enough, the dominant contribution to the compressibility will be from the condensate. By measuring the compressibility, we can measure the parameter c' .

3. μ

Knowing the value of c' , the value of μ is quite straightforward to measure. It can be related to the density of

atoms within the condensate, using the relation

$$n_0 = \sqrt{\frac{\mu}{2c'}} \quad (\text{A5})$$

4. c_2

c_2 is a static parameter and should be measurable from static properties, for example, the spin susceptibility. The terms in the free energy involving the magnetization can be rewritten as $c_2 M_z^2 + h M_z$, where h is the magnetic field along z . The spin susceptibility is approximately h/c_2 , from which we can deduce c_2 . In most practical cases at low temperature, the value of c_2 is not very different from that obtained from the atomic s wave scattering rates.

5. Γ_2

The mode $\phi_{+1} + \phi_{-1}$ will have an oscillatory component and also a part that is decaying. The value of the

oscillation frequency can be shown to be $(1 + \sqrt{5})\Gamma_2 c_2 n_0$. If we know the value of c_2 from static experiments, we can obtain the value of Γ_2 .

6. c_0 and γ

We have shown that $c_0 + C\gamma^2$ can be determined by measuring c' . To disentangle the two quantities, we look at the second sound velocity. The equation for the second sound velocity is

$$c_s = \sqrt{\frac{g_0^2 n_0}{C} + 2\Gamma_2^2 (c' + \frac{g_0 \gamma}{\Gamma_2}) n_0} \quad (\text{A6})$$

If we know c_s , the only unknown variable is γ . Having obtained γ from this equation, we can calculate c_0 , from the known value of c' .

The authors wish to acknowledge conversations with D. A. Huse, A. Lamacraft, S. Leslie, D. Podolsky, L. Sadler, D. M. Stamper-Kurn, M. Vengalattore and A. Vishwanath, and support from DOE (S. M.), NSF DMR-0238760 (C. X. and J. E. M.), and the IBM SUR program.

-
- ¹ A. Gorlitz et al., Phys. Rev. Lett. **90**, 090401 (2003).
² D. S. Hall, M. R. Matthews, C. E. Wieman, and E. A. Cornell, Phys. Rev. Lett. **81**, 1543 (1988).
³ L. Sadler, J. M. Higbie, S. R. Leslie, M. Vengalattore, and D. M. Stamper-Kurn, Nature **443**, 312 (2006).
⁴ Z. Hadzibabic, P. Kruger, M. Cheneau, B. Battelier, and J. Dalibard, Nature **441**, 1118 (2006).
⁵ T.-L. Ho, Phys. Rev. Lett. **81**, 742 (1998).
⁶ E. Demler and F. Zhou, Phys. Rev. Lett. **88**, 163001 (2002).
⁷ J. Mur-Petit, M. Guilleumas, A. Polls, A. Sanpera, M. Lewenstein, K. Bongs, and K. Sengstock, Phys. Rev. A **73**, 013629 (2006).
⁸ A. Lamacraft, cond-mat/0611017.
⁹ S. Mukerjee, C. Xu, and J. E. Moore, Phys. Rev. Lett. **97**, 120406 (2006).
¹⁰ H. Saito and Y. K. M. Ueda, Phys. Rev. A **75**, 013621 (2007).
¹¹ H. Saito and Y. K. M. Ueda, arXiv:0704.1377.
¹² P. C. Hohenberg and B. I. Halperin, Rev. Mod. Phys. **49**, 435 (1977).
¹³ H. Pu, C. K. Law, S. Raghavan, J. H. Eberly, and N. P. Bigelow, Phys. Rev. A **60**, 1463 (1999).
¹⁴ N. P. Robins, W. Zhang, E. A. Ostrovskaya, and Y. S. Kivshar, Phys. Rev. A **64**, 021601 (2001).
¹⁵ H. Saito and M. Ueda, Phys. Rev. A **72**, 023610 (2005).
¹⁶ W. Zhang, D. L. Zhou, M.-S. Chang, M. S. Chapman, and L. You, Phys. Rev. Lett. **95**, 180403 (2005).
¹⁷ A. J. Leggett, Rev. Mod. Phys. **73**, 307 (2001).
¹⁸ D. Podolsky, A. Vishwanath, and S. Chandrasekharan, unpublished.
¹⁹ P. Olsson, Phys. Rev. Lett. **75**, 2758 (1995).
²⁰ B. I. Halperin and P. C. Hohenberg, Phys. Rev. **188**, 898 (1969).
²¹ P. W. Anderson, Rev. Mod. Phys. **38**, 298 (1966).
²² L. P. Pitaevskii, Sov. Phys. – JETP **8**, 282 (1959).
²³ A. J. Bray, Adv. Phys. **51**, 481 (1994).
²⁴ D. A. Huse, Phys. Rev. B **34**, 7845 (1986).
²⁵ K. Damle, S. N. Majumdar, and S. Sachdev, Phys. Rev. A **54**, 5037 (1996).